

Transverse Charge Densities

GERALD A. MILLER

Department of Physics, University of Washington, Seattle, WA 98195-1560,
USA

Key Words Electromagnetic form factors, transverse charge densities, transverse momentum distributions, generalized parton distributions

Abstract Electromagnetic form factors have long been used to probe the underlying charge and magnetization densities of hadrons and nuclei. Traditional three-dimensional Fourier transform methods are not rigorously applicable for systems with constituents that move relativistically. The use of the transverse charge density is a new, rigorously defined way to analyze electromagnetic form factors of hadrons. This review is concerned with the following issues: what is a transverse charge density; how is one extracted one from elastic scattering data; the existing results; what is the relationship with other observable quantities; and, future prospects.

CONTENTS

INTRODUCTION	2
<i>Electromagnetic form factors are not three-dimensional Fourier transforms of charge densities</i>	3
<i>What is a transverse charge density?</i>	6
<i>Simple example</i>	9
ZOO OF NUCLEON DISTRIBUTIONS AND DENSITIES	11

arXiv:1002.0355v1 [nucl-th] 1 Feb 2010

SINGULAR PIONIC TRANSVERSE CHARGE DENSITY	16
NUCLEON TRANSVERSE CHARGE DENSITIES	20
<i>Meaning of central density $b = 0$</i>	23
<i>Inclusive-exclusive Connection Interpretation of the negative neutron charge density</i>	24
<i>Magnetization Density</i>	25
<i>Non-cylindrically symmetric transverse charge density and shape of the nucleon</i>	28
TRANSVERSE TRANSITION CHARGE DENSITIES	30
NUCLEAR TRANSVERSE CHARGE DENSITIES	31
<i>Other Applications</i>	32
SUMMARY AND FUTURE DIRECTIONS	33
ACKNOWLEDGMENTS	34

1 INTRODUCTION

A truly impressive level of experimental technique, effort and ingenuity has been applied to measuring the electromagnetic form factors of the proton, neutron (nucleon) and pion (1, 2, 3, 4). These quantities are probability amplitudes that a given hadron can absorb a specific amount of momentum and remain in the ground state, and therefore should supply information about charge and magnetization densities. The text-book interpretation of these form factors is that their Fourier transforms are measurements of the charge and magnetization densities. This interpretation is deeply buried in the thinking of nuclear and particle physicists and continues to guide intuition, as it has since the days of the Nobel prize-winning work of Hofstadter(5). Nevertheless, the relativistic motion of the constituents of the system causes the text-book interpretation to be incorrect (6).

The preceding statement leads to several questions, the first being: Is the statement correct? If correct, how fast do the constituents actually have to move to violate the non-relativistic interpretation? Why is it that the motion of the constituents and not that of the entire system that is relevant? The answers to these questions are probably displayed within the existing literature. However, obtaining general clear answers has been sufficiently difficult that posing even the first question of this paragraph would not lead to a unanimous answer. Moreover, there is another more important question. If the non-relativistic approach is not correct: What is the correct procedure to determine model-independent information regarding hadronic charge and magnetization densities? How should we interpret the beautifully precise electromagnetic form factor data being produced at Jefferson Laboratory, Bates, Bonn and Mainz?

The aim of this review is to present and clarify answers to these questions. The most immediate question is addressed here. The only way to determine model-independent information about the charge distribution is to study the transverse charge density $\rho(b)$ (7) which gives the density of a hadron moving at infinite momentum at a transverse (to the direction of rapid motion) distance b from the transverse center of momentum. It is only in the infinite momentum frame that one can define such a center. Information about the charge density in terms of longitudinal coordinates is not yet available in a meaningful way.

1.1 Electromagnetic form factors are not three-dimensional Fourier transforms of charge densities

Physicists are trained to believe that physics is independent of the inertial reference frame. In non-relativistic quantum mechanics this invariance allows us

to express the wave function as a product of a plane-wave factor (that describes the motion of the center of mass) with a function that depends only on internal relative coordinates. Thus for two spinless particles:

$$\Psi(\vec{r}_1, \vec{r}_2) = e^{i\vec{P}\cdot\vec{R}}\phi(\vec{r}), \quad (1)$$

where \vec{P} is the total momentum, \vec{R} is the position of the com, and $\vec{r} = \vec{r}_1 - \vec{r}_2$. Then the non-relativistic form factor $F_{NR}(|\vec{q}|)$, which is the probability amplitude for the system to absorb a momentum \vec{q} and remain in its initial state, is given by the integral

$$F_{NR}(|\vec{q}|) = \int d^3r |\phi(\vec{r})|^2 e^{i\vec{q}\cdot\vec{r}/2}, \quad (2)$$

if the masses of the two constituents are the same. One sees that the square of a wave function or probability density is being probed.

However the separation appearing in Eq. (1) is not generally valid. For a similar but relativistic system the Minkowski-space, Bethe-Salpeter wave function $\Phi(k, P)$ (where k is the relative four-momentum and P is the total four-momentum) can be written in a compact form if the interaction kernel is given by a set of Feynman graphs (8,9), using the Nakanishi integral representation:

$$\Phi(k; P) = -\frac{i}{\sqrt{4\pi}} \int_{-1}^1 dz \int_0^\infty d\gamma \frac{g(\gamma, z)}{\left[\gamma + m^2 - \frac{1}{4}M^2 - k^2 - P \cdot k z - i\varepsilon\right]^3}, \quad (3)$$

where m is the mass of each constituent scalar particle and M is the hadronic mass. The weight function $g(\gamma, z)$ itself is not singular, but the singularities of the BS amplitude are reproduced by using Eq. (3) (10). The key feature of Eq. (3) is that the covariant wave function depends explicitly on the total four-momentum P . Another way of presenting the contents of Eq. (3) involves the relativistic boost operator used to obtain the wave function in a moving frame from one in

which the hadron is at rest. The Nakanishi representation allows one to perform the boost merely by changing the value of P .

The explicit dependence on P dramatically influences our understanding of form factors because the initial and final hadrons have different momentum and therefore different wave functions. The presence of different wave functions of the initial and final nucleons invalidates a naive probability or density interpretation.

Assuming that only one of the scalar constituents carry charge, the electromagnetic form factor is obtained by evaluating the impulse approximation triangle diagram, with the result (10).

$$(P + P')^\mu F(Q^2) = i \int \frac{d^4 k}{(2\pi)^4} (P + P' + k)^\mu (k^2 - m^2) \Phi(\frac{1}{2}P - k, P) \Phi(\frac{1}{2}P' - k, P'), \quad (4)$$

where $P' = P + q$.

The form factor of Eq. (4) seems to differ markedly from the usual non-relativistic expression Eq. (2), expressed in terms of momentum space wave functions $\tilde{\phi}$:

$$F^{NR}(|\vec{q}|) = \int \frac{d^3 k}{(2\pi)^3} \tilde{\phi}^*(\vec{k} + \vec{q}/2) \tilde{\phi}(\vec{k}). \quad (5)$$

It is comforting that in the non-relativistic limit, defined by the replacement

$$x = \frac{k^0 + k^3}{P^0 + P^3} \rightarrow \frac{1}{2} + \frac{k^3}{2m}, \quad M - 2m \ll 2m, \quad (6)$$

the IMF, light-front wave function becomes identical to the rest frame instant-form wave function (11). This means (6) that if the condition Eq. (6) is true for a given model, then Eq. (5) (and therefore Eq. (2)) is obtained from Eq. (4). In this case, one may extract $\rho(\mathbf{r}) \equiv |\tilde{\phi}(\mathbf{r})|^2$ from a three-dimensional Fourier transform of F_{NR} . However, the conditions Eq. (6) are not expected to be obtained for hadrons, although they are valid for nuclei (6). Furthermore, if the charged particles of a given system have different masses, one obtains (in the non-relativistic

limit for all constituents)

$$F^{NR}(\vec{q}) = \int d^3r \sum_i \rho_i(\vec{r}) e^{-i\vec{q}\cdot\vec{r}m_i/M}, \quad (7)$$

where ρ_i, m_i are the charge density and mass of the i 'th constituent, and one can not obtain the charge density from the form factor.

1.2 What is a transverse charge density?

A proper determination of a charge density requires the measurement of a matrix element of a density operator. We show here that measurements of the hadronic form factor directly involve the three-dimensional charge density of partons in the infinite momentum frame, $\hat{\rho}_\infty(x^-, \mathbf{b})$. Before discussing this quantity we need to provide a brief introduction to light-cone coordinates.

In the infinite momentum frame IMF the time coordinate $ct = x^0/\sqrt{2}$ is expressed in a frame moving along the negative z direction with a velocity nearly that of light using the Lorentz transformation as the variable $x^+ = (x^0 + x^3)/\sqrt{2}$, with the usual γ factor is absorbed by a Jacobean of an integral over volume (12). The x^+ variable is canonically conjugate to the minus-component of the momentum operator $p^- \equiv (p^0 - p^3)/\sqrt{2}$. The longitudinal spatial variable is $x^- = (x^0 - x^3)/\sqrt{2}$ and its conjugate momentum is $p^+ = (p^0 + p^3)/\sqrt{2}$. It is this plus-component of momentum that is associated with the usual Bjorken variable. The transverse coordinates x, y are written as \mathbf{b} with the conjugate \mathbf{p} . In the literature, these transverse coordinates are sometimes written with a subscript \perp , but here we shall simply use boldface to denote the transverse components of position and momentum vectors. We shall also always use a light-front time quantization which sets x^+ and the plus-component of all spatial variables to zero. This means that x^- can be thought of as the longitudinal variable $-\sqrt{2}x^3$. One

extremely useful aspect of using these variables is that Lorentz transformations to frames moving with different transverse velocities do not depend on interactions. These transformations form the kinematic subgroup of the Poincaré group so that boosts in the transverse direction are accomplished using the transverse component of the position operator (as in the non-relativistic theory).

In the IMF, the electromagnetic charge density J^0 becomes J^+ and

$$\hat{\rho}_\infty(x^-, \mathbf{b}) = J^+(x^-, \mathbf{b}) = \sum_q e_q \bar{q}(x^-, \mathbf{b}) \gamma^+ q(x^-, \mathbf{b}) = \sum_q e_q \sqrt{2} q_+^\dagger(x^-, \mathbf{b}) q_+(x^-, \mathbf{b}), \quad (8)$$

where $q_+(x^\mu) = \gamma^0 \gamma^+ / \sqrt{2} q(x^\mu)$, the independent part of the quark-field operator $q(x^\mu)$. The time variable, x^+ is set to zero. Note the appearance of the absolute square of quark field-operators, which is the signature of a true density.

We are concerned with the relationship between charge density and the electromagnetic form factor $F(Q^2)$, determined from the current density via

$$F(Q^2) = \frac{\langle p'^+, \mathbf{p}' | J^+(0) | p^+, \mathbf{p} \rangle}{2p^+}, \quad (9)$$

where the normalization is $\langle p'^+, \mathbf{p}' | p^+, \mathbf{p} \rangle = 2p^+ (2\pi)^3 \delta(p'^+ - p^+) \delta^{(2)}(\mathbf{p}' - \mathbf{p})$. Spin or helicity dependence is ignored in the present sub-section. We take the momentum transfer $q_\alpha = p'_\alpha - p_\alpha$ to be space-like, with the square of the space-like four-momentum transfer $q^2 = -Q^2$ and use the Drell-Yan (DY) frame with $(q^+ = 0, Q^2 = \mathbf{q}^2)$. No longitudinal momentum is transferred, so that initial and final states are related only by kinematic transformations. Moreover, with this condition the current operator links Fock-state components with the same number of constituents. The matrix element appearing in Eq. (9) involves the combination of creation and destruction operators: $b^\dagger b - d^\dagger d$ for each flavor of quark, so that the valence charge density is probed. The form factor F is independent of renormalization scale because the vector current $\bar{q} \gamma^\mu q$ is conserved (13).

The spatial structure of a hadron can be examined using states that are transversely localized (7, 14, 13) through a linear superposition

$$|p^+, \mathbf{R} = \mathbf{0}\rangle \equiv \mathcal{N} \int \frac{d^2\mathbf{p}}{(2\pi)^2} |p^+, \mathbf{p}\rangle, \quad (10)$$

where \mathcal{N} is a normalization factor satisfying $|\mathcal{N}|^2 \int \frac{d^2\mathbf{p}}{(2\pi)^2} = 1$. Wave packet representations can be used to avoid states normalized to δ functions (15, 16), but this leads to the same results as using Eq. (10). Considering $2p^+p^- - \mathbf{p}^2 = m_\pi^2 > 0$, (with $p^- > 0$) one finds p^+ must be very large because the range of integration over \mathbf{p} is large. Using such an ultra-large or infinite value of p^+ , maintains the interpretation of a pion moving in the IMF with well defined longitudinal momentum (15). It is in just such an infinite momentum that the parton interpretation of a hadron is valid. Setting the transverse center of momentum to zero, Eq. (10), allows a meaningful transverse distance \mathbf{b} . A Fock-space parton representation of the position of the transverse center of momentum, \mathbf{R} , provides a useful relation between longitudinal momentum fractions and transverse positions (14):

$$\mathbf{R} = \sum_i x_i \mathbf{b}_i, \quad (11)$$

where the sum is over the finite number of constituents in a given component.

Next we relate the charge density

$$\rho_\infty(x^-, \mathbf{b}) = \frac{\langle p^+, \mathbf{R} = \mathbf{0} | \hat{\rho}_\infty(x^-, \mathbf{b}) | p^+, \mathbf{R} = \mathbf{0} \rangle}{\langle p^+, \mathbf{R} = \mathbf{0} | p^+, \mathbf{R} = \mathbf{0} \rangle}, \quad (12)$$

to $F(Q^2)$. In the DY frame no momentum is transferred in the plus-direction, so that information regarding the x^- dependence of the density is not accessible. Therefore we integrate over x^- , using the relationship $q_+^\dagger(x^-, \mathbf{b})q_+(x^-, \mathbf{b}) = e^{i\hat{p}^+x^-} e^{-i\hat{\mathbf{p}}\cdot\mathbf{b}} q_+^\dagger(0)q_+(0)e^{i\hat{\mathbf{p}}\cdot\mathbf{b}} e^{-i\hat{p}^+x^-}$, to find

$$\rho(b) \equiv \int dx^- \rho_\infty(x^-, \mathbf{b}) = \langle p^+, \mathbf{R} = \mathbf{0} | \hat{\rho}_\infty(0, \mathbf{b}) | p^+, \mathbf{R} = \mathbf{0} \rangle / (2p^+). \quad (13)$$

The use of Eq. (9) and the expansion Eq. (10) leads to the simplification of the right-hand-side of the above equation:

$$\rho(b) = \int \frac{d^2q}{(2\pi)^2} F(Q^2 = \mathbf{q}^2) e^{-i\mathbf{q}\cdot\mathbf{b}}, \quad (14)$$

where $\rho(b)$ is termed the transverse charge density, giving the charge density at a transverse position b , irrespective of the value of the longitudinal position or momentum. The use of a three-dimensional coordinate space density $\hat{\rho}_\infty(x^-, \mathbf{b})$ to obtain the transverse density appeared in Ref. (17). Previous derivations (7, 14, 13, 18) used a density operator involving transverse position and longitudinal momentum variables; see sect. 2.

If the non-relativistic (NR) limit Eq. (6) is valid, one finds that (6)

$$\rho^{NR}(b) = \int_{-\infty}^{\infty} dz \rho(r), \quad (15)$$

where $\rho(r)$ is the square of the wave function obtained from Eq. (2). This, as well as the integral over the longitudinal coordinate that appears in Eq. (13), illustrates the nature of the transverse density as a reduction of the three-dimensional density. Moreover, these integrals appear in the Glauber theory (19) of high energy scattering in which scattering amplitudes are expressed in terms of transverse densities. A recent example is found in (20).

1.3 Simple example

It is worthwhile to use a simple example (6) in which a scalar particle Ψ is modeled as a bound state of two different scalar particles ξ, χ , with a point-like coupling such that the interaction Lagrangian is $g\Psi\xi\chi$. Then the Bethe-Salpeter wave function is obtained from Eq. (3) by replacing $g(\gamma, z)/\sqrt{4\pi}$ by the simple coupling-constant g . The explicit Bethe-Salpeter wave function can then be obtained by

straightforward integration and found to be proportional to the product of Klein-Gordan propagators. For this model, the evaluation of the form factor Eq. (4) can be performed in three different ways. One can simply evaluate the Feynman integral, one can take work in the IMF with $P^3 \rightarrow \infty$ (21) or one can proceed by first integrating over k^- . The resulting form factor is the same in all three cases (6). The form factor can be expressed in terms of a three-dimensional integral which involves a light-front wave function: $\psi(x, \boldsymbol{\kappa})$

$$\psi(x, \boldsymbol{\kappa}) \equiv g \left[M^2 - \frac{\boldsymbol{\kappa}^2 + m_1^2}{x} - \frac{\boldsymbol{\kappa}^2 + m_2^2}{1-x} \right]^{-1}. \quad (16)$$

In that case

$$F(Q^2) = \frac{1}{2(2\pi)^3} \int d^2\boldsymbol{\kappa} \int_0^1 \frac{dx}{x(1-x)} \psi^*(x, \boldsymbol{\kappa} + (1-x)\mathbf{q}) \psi(x, \boldsymbol{\kappa}). \quad (17)$$

The relative variables are $x, \boldsymbol{\kappa}$ with $x = k^+/P^+$ and $\boldsymbol{\kappa} = \boldsymbol{\kappa}_1 - \boldsymbol{\kappa}_2$. The function $\psi(x, \boldsymbol{\kappa})$ can be obtained from Φ of Eq. (3) by integrating over k^- (22, 23, 11).

One can obtain a relation between the form factor and a coordinate space density, by expressing the light-front wave function $\psi(x, \boldsymbol{\kappa})$ in terms of the canonically conjugate spatial variable $\mathbf{B} = \mathbf{b} - \mathbf{b}_2$, where \mathbf{b} is the transverse position operator of the charged constituent. Then $\tilde{\psi}(x, \mathbf{B}) = \int \frac{d^2\boldsymbol{\kappa}}{(2\pi)^2} e^{i\boldsymbol{\kappa}\cdot\mathbf{B}} \psi(x, \boldsymbol{\kappa})$, and

$$F(Q^2) = \frac{1}{4\pi} \int d^2\mathbf{B} \int_0^1 \frac{dx}{x(1-x)} |\tilde{\psi}(x, \mathbf{B})|^2 e^{-i\mathbf{B}(1-x)\cdot\mathbf{q}}. \quad (18)$$

We express the form factor in terms of the position of the charged constituent by using the condition that the center of transverse momentum is set to zero (Eq. (11) with two components): $\mathbf{R} = 0 = x\mathbf{b} + (1-x)\mathbf{b}_2$ so that $\mathbf{B} = \mathbf{b}/(1-x)$.

Expressing the form factor in terms of \mathbf{b} gives

$$F(Q^2) = \frac{1}{4\pi} \int d^2\mathbf{b} \int_0^1 \frac{dx}{x(1-x)^3} |\tilde{\psi}(x, \frac{\mathbf{b}}{1-x})|^2 e^{-i\mathbf{b}\cdot\mathbf{q}}. \quad (19)$$

Comparing with Eq. (14) allows us to identify the transverse density as

$$\rho(b) = \pi \int_0^1 \frac{dx}{x(1-x)^3} |\tilde{\psi}(x, \frac{\mathbf{b}}{1-x})|^2, \quad (20)$$

which for the present model is evaluated as

$$\rho(b) = \frac{g^2}{2(2\pi)^3} \int_0^1 dx \frac{x}{(1-x)} K_0^2(\sqrt{m^2 - M^2 x(1-x)} \frac{b}{1-x}). \quad (21)$$

The mass M must be less than $2m$ for the hadron Ψ to be stable. We define a positive binding fraction ϵ , so that $M = 2m - \epsilon m$ ($0 < \epsilon < 2$). Small values of ϵ correspond to the applicability of the non-relativistic limit. The transverse densities of Eq. (20) results are shown in Fig. 1, for $\epsilon = 0.01$ and 0.1 . As expected from non-relativistic intuition, the smaller value of the binding energy corresponds to a greater spatial extent.

2 ZOO OF NUCLEON DISTRIBUTIONS AND DENSITIES

The vast literature concerning the distribution functions that are used to describe nucleon structure includes generalized parton distributions GPDs (24, 25, 26, 27, 28, 29, 30, 31, 32, 33, 34, 35) and transverse momentum distributions (36, 37, 38, 39, 40, 41, 42). The relationship between GPDs, transverse charge densities and TMDs is discussed in the present section.

We begin by discussing generalized parton distributions, GPDs and follow the discussion of Burkardt (14). Deep-inelastic scattering experiments allow the determination of parton distribution functions (PDFs), which give the probability that quarks carry a given fraction x of the nucleon longitudinal (+)momentum in the infinite momentum frame (IMF). PDFs are the forward matrix element of a light-like correlation function,

$$q(x) = \langle P, S | \hat{O}_q(x, \mathbf{0}) | P, S \rangle \quad (22)$$

with

$$\hat{O}_q(x, \mathbf{0}) \equiv \int \frac{dx^-}{4\pi} \bar{q}\left(-\frac{x^-}{2}, \mathbf{0}\right) \gamma^+ q\left(\frac{x^-}{2}, \mathbf{0}\right) e^{ixp^+ x^-}, \quad (23)$$

where $|P, S\rangle$ represents the wave function. Here we use the light-cone gauge $A^+ = 0$. The use of the canonical field expansion for the quark field-operators shows explicitly that PDFs give the probability that the quarks carry a longitudinal momentum fraction x . We do not display the scale dependence of the PDFs to simplify the notation.

Generalized parton distributions (GPDs)(24,25,26,27,28,29,30,31,32,33,34,35) which describe the scaling limit in real and virtual Compton scattering experiments, are defined by allowing the momenta and spins of the initial and final nucleons to differ:

$$\langle P', S' | \hat{O}_q(x, \mathbf{0}_\perp) | P, S \rangle \quad (24)$$

$$= \frac{1}{2\bar{p}^+} \bar{u}(P', s') \left(\gamma^+ H_q(x, \xi, t) + i \frac{\sigma^{+\nu} \Delta_\nu}{2M} E_q(x, \xi, t) \right) u(P, s) \quad (25)$$

with $\bar{p}^\mu = \frac{1}{2}(P^\mu + P'^\mu)$ being the mean momentum of the target, $\Delta^\mu = P'^\mu - P^\mu$ the four momentum transfer, and $t = \Delta^2$ the invariant momentum transfer. The skewedness parameter $\xi = -\frac{\Delta^+}{2\bar{p}^+}$ represents the change in the longitudinal component of the nucleon momentum.

GPDs allow for a unified description of a number of hadronic properties. If $P' = P$, the forward limit, they reduce to conventional parton distribution functions $H_q(x, 0, 0) = q(x)$. The integral over x causes the x^- coordinate to vanish, so that the operator \hat{O}_q is converted into a local current operator and results in the appearance of the usual Dirac form factors of the nucleon

$$\sum_q e_q \int dx H_q(x, \xi, t) = F_1(t) \quad (26)$$

$$\sum_q e_q \int dx E_q(x, \xi, t) = F_2(t). \quad (27)$$

The next step is to define impact parameter parton distributions (14). One localizes the nucleon in the transverse direction using the superposition Eq. (10) but with light-cone helicity states (43) $|P^+, \mathbf{p}, \lambda\rangle = |P, S\rangle$. For a transversely localized state $|p^+, \mathbf{R}_\perp = \mathbf{0}_\perp, \lambda\rangle$, Burkardt's impact parameter dependent PDF is given by

$$q(x, \mathbf{b}) \equiv \left\langle p^+, \mathbf{R}_\perp = \mathbf{0}_\perp, \lambda \left| \hat{O}_q(x, \mathbf{b}) \right| p^+, \mathbf{R}_\perp = \mathbf{0}_\perp, \lambda \right\rangle. \quad (28)$$

The operator $\hat{O}_q(x, \mathbf{b})$ is obtained by a translation of the operator appearing in Eq. (23) in the transverse plane

$$\hat{O}_q(x, \mathbf{b}) = \int \frac{dx^-}{4\pi} \bar{q}\left(-\frac{x^-}{2}, \mathbf{b}\right) \gamma^+ q\left(\frac{x^-}{2}, \mathbf{b}\right) e^{ixp^+x^-}. \quad (29)$$

The function $q(x, \mathbf{b})$ gives the probability density that a quark of momentum fraction x is located at a transverse position \mathbf{b} .

Burkardt (14) used the transversely localized states of the same helicity to show that $q(x, \mathbf{b})$ is the two-dimensional Fourier transform of the GPD H_q :

$$q(x, \mathbf{b}) = \int \frac{d^2q}{(2\pi)^2} e^{-i \mathbf{q} \cdot \mathbf{b}} H_q(x, t = -\mathbf{q}^2). \quad (30)$$

Integration over x using Eq. (26) and Eq. (14) shows that

$$\rho(b) = \int dx \sum_q e_q q(x, \mathbf{b}) = \int \frac{d^2q}{(2\pi)^2} F_1(t = -\mathbf{q}^2) e^{-i \mathbf{q} \cdot \mathbf{b}}. \quad (31)$$

This means that the transverse density can be obtained either as an integral over x of $q(x, b)$ or as an integral over x^- of the three dimensional coordinate space density, as in Sect. 1.2. This equality of an integral over a momentum with one over a distance is an example of Parseval's theorem. In either case, model-independent information regarding the longitudinal coordinate is not available because the probe momentum is transverse. That is $q^+ = 0$.

In the model of Sect. 1.3 (scalar hadron made of two scalar constituents), $q(x)$ can be obtained from the integrand of Eq. (20) as

$$q(x, b) = \frac{\pi}{x(1-x)^3} \left| \tilde{\psi}\left(x, \frac{\mathbf{b}}{1-x}\right) \right|^2. \quad (32)$$

One sees, for large values of x approaching unity, that the transverse extent is very narrow because this corresponds to very large values of the relative transverse separation $\mathbf{B} = \mathbf{b}/(1-x)$ for finite values of \mathbf{b} . Thus the transverse spatial extent depends explicitly on the value of x . In particular, large values of x are associated with small values of b .

Transverse momentum distributions TMDs are another generalization of parton distribution functions. These, which contain probability distributions regarding both the longitudinal momentum fraction x and transverse momentum \mathbf{k} carried by the quarks, are given by (36, 37, 40)

$$\Phi_q^\Gamma(x = \frac{k^+}{P^+}, \mathbf{k}) = \langle P, S | \int \frac{d\zeta^- d^2\boldsymbol{\zeta}}{2(2\pi)^3} e^{i(k^+\zeta^- - \mathbf{k}\cdot\boldsymbol{\zeta})} \bar{q}(0)\Gamma q(\zeta^-, \boldsymbol{\zeta}) | P, S \rangle, \quad (33)$$

where the time separation $\zeta^+ = 0$. Here the quark field operators are the gauge invariant operators in gauges for which the gauge potentials vanish at space-time infinity (44, 45). These operators are necessary for non-zero transverse spatial separations, $\boldsymbol{\zeta}$. The operator Γ is a Dirac matrix that defines the quark density.

The initial and final states appearing in Eq. (33) have the same momentum; the major difference between TMDs and GPDs. Another major difference is that GPDs involve densities in transverse coordinate space, but TMDs involve densities in transverse momentum space. However, one can use Wigner distributions (44) to show that GPDs and TMDs are obtained from different manipulations on the same operator. We define the reduced Wigner distribution as

$$W_q^\Gamma(\zeta^-, \boldsymbol{\zeta}, k^+, \mathbf{k}) = \frac{1}{4\pi} \int d\eta^- d^2\boldsymbol{\eta} e^{ik^+\eta^- - i\mathbf{k}\cdot\boldsymbol{\eta}} \bar{q}(\zeta^- - \eta^-/2, \boldsymbol{\zeta} - \boldsymbol{\eta}/2) \Gamma q(\zeta^- + \eta^-/2, \boldsymbol{\zeta} + \boldsymbol{\eta}/2).$$

GPDs are obtained by taking the matrix element of $W_q^\Gamma(\zeta^- = 0, \zeta = \mathbf{0}, k^+, \mathbf{k})$ between states of different momentum and then integrating over \mathbf{k} as in

$$H_q(x, \xi, t) = \langle P', S | \int \frac{d^2\mathbf{k}}{(2\pi)^2} W_q^{\gamma^+}(\xi^-, \zeta, k^+, \mathbf{k}) | P, S \rangle, \quad (35)$$

and TMDs are obtained by taking the matrix element of $W_q^\Gamma(\zeta^-, \zeta, k^+, \mathbf{k})$ between states of the very same momentum:

$$\Phi_q^\Gamma(x, \mathbf{k}) = \langle P, S | \int \frac{d\zeta^-}{(2\pi)^2} W_q^\Gamma(\zeta^-, \zeta, k^+, \mathbf{k}) | P, S \rangle. \quad (36)$$

2.0.1 *x*-SUM RULES, THE CONNECTION TO THE EQUAL TIME FORMALISM, AND LATTICE CALCULATIONS The integral of a GPD over all values of x as in Eq. (26) and Eq. (27) converts the non-local bilinear appearing in Eq. (29) into a local operator. More generally, the GPD is a correlation function of quarks at the same light cone time $x^+ = 0$. The integral over x gives also $x^- = 0$, so that both the time t and spatial z separations vanish. Thus one can compare matrix elements involving the integral over x with related matrix elements computed using the equal time formalism, $t = 0$. Moreover, performing the x integral allows a connection with lattice QCD calculations. The lattice formulation is built using covariant Euclidean space. If one sets it and z to 0 in a lattice calculation one obtains a quantity that depends on transverse coordinates suitable for comparison with a relevant transverse experimentally measured quantity. This relation has been pointed out in connection with transversity observables in Ref. (46) and used in Refs. (47, 48, 49, 50).

A similar connection (51) between the light-front and equal time formalism occurs when using TMDs. A TMD Eq. (33) gives the probability that a quark has a three momentum characterized by (x, \mathbf{k}) . The relevant matrix element involves quarks separated at the same light-cone time $\zeta^+ = 0$. Integration over

x sets also ζ^- to 0, so one obtains a density evaluated using quarks at the same time.

3 SINGULAR PIONIC TRANSVERSE CHARGE DENSITY

Understanding the pion is necessary to learn how QCD describes the interaction and existence of elementary particles. As a nearly massless excitation of the QCD vacuum with pseudoscalar quantum numbers, the pion plays a central role in nuclear and particle physics as the carrier of the longest ranged force between nucleons and as a harbinger of spontaneous symmetry breaking.

Computing the electromagnetic form factor of the pion, $F_\pi(Q^2)$, at asymptotically large values of Q^2 from first principles was one of the early challenges to using perturbative QCD in exclusive processes (52, 53, 54, 55). Such calculations have been extended (56, 57, 58, 59) by including effects of higher order in the strong coupling constant and higher twist effects. The lowest order results are about a factor of three smaller than existing data, and higher order and higher twist effects are not small at currently available values of Q^2 (59). It is widely believed that at large enough values of momentum transfer Q^2 the leading-order perturbative formula will be correct, but these large values may be very large indeed (60). As a result there is considerable experimental interest in determining the transition to the region where perturbative QCD can be applied. New measurements (61, 62) have been performed and more are planned (63). Here we review the first analysis (17) that provided a model-independent pionic transverse charge density.

Recent pion data (61, 62) provide a very accurate measurement of the longitudinal part of the electroproduction cross section and the related pion form factor

up to a value of $Q^2 = 2.45 \text{ GeV}^2$. The result is that existing data for the pion form factor are well represented by the monopole form

$$F_\pi(Q^2) = 1/(1 + R^2 Q^2/6), \quad (37)$$

with $R^2 = 0.431 \text{ fm}^2$. The expression Eq. (37) allows one to determine the transverse density from Eq. (14) with the result:

$$\rho(b) = \frac{3K_0\left(\frac{\sqrt{6}b}{R}\right)}{\pi R^2}, \quad (38)$$

where K_0 is modified Bessel function of rank zero. For small values of b this function diverges as $\sim \log(b)$, hence the transverse density is singular and infinite at the origin. This infinity is not to be “cured” by a renormalization procedure because the charge density under consideration is the matrix element of a valence quark operator between eigenstates of the full Hamiltonian. Furthermore, divergences of quark distribution functions that occur at small values of Bjorken x do not occur here because transverse charge density involves the difference between quark and anti-quark densities. Many field theory models, derived even before QCD was established (64) obtain a form factor that corresponds to a divergent transverse density. Note also that any model, such as vector meson dominance or holographic QCD (65, 66, 67) yielding a monopole form factor has a central density with a logarithmic divergence. Thus holographic QCD does not supply a representation of the soft component (60) of the pion wave function.

Intuition regarding a possible singularity in the central charge density may be gained from other examples. Suppose that the non-relativistic (NR) limit in which the quark masses are heavy is applicable. Then the pion would be a pure $q\bar{q}$ object and the charge density would be the Fourier transform of the form factor (Sect. 1.1). Given the form factor of Eq. (37) the NR three-dimensional

density would be uniquely given by

$$\rho_{\text{NR}}(r) = \frac{3}{2\pi r R^2} e^{-\frac{\sqrt{6}r}{R}}, \quad (39)$$

where r is the distance relative to the pion center of mass. This density diverges at $r = 0$. If one takes $r = \sqrt{b^2 + z^2}$ as demanded by the rotational invariance of the non-relativistic wave function, then one finds from Eq. (15) that the non-relativistic transverse charge density takes the form of $\rho(b)$ of Eq. (38).

The divergence of the central transverse charge density encountered here may be the consequence of using a simple parametrization, presently untested by measurements at larger values of Q^2 . Thus we examine other approaches. Consider first perturbative QCD (pQCD), which provides a prediction (52)-(55) for asymptotically large values of Q^2 that

$$\lim_{Q^2 \rightarrow \infty} F_\pi(Q^2) = 16\pi\alpha_s(Q^2)f_\pi^2/Q^2, \quad (40)$$

with the pion decay constant $f_\pi = 93$ MeV, and in leading order:

$$\alpha_s(Q^2) = \frac{4\pi}{(11 - \frac{2}{3}n_f) \ln \frac{Q^2}{\Lambda^2}}, \quad (41)$$

with n_f the number of quarks of mass smaller than Q and Λ is a parameter fixed by data. The $\log Q^2$ term in the denominator does not lead to a non-singular behavior of $\rho(b)$ for small values of b because $\rho(b) \sim \log \log \frac{1}{b}$ and the pQCD form factor corresponds to a singularity at short distance. This singularity would arise in any model form factor even one based on sum rules *e.g.* (60) that approaches the pQCD asymptotically.

Chiral quark models (see the review (68)) present other models (69, 70) of transverse charge densities that are singular at the center as $\log b$ because the pion form factor takes the monopole form. It is nevertheless interesting to note

that each and every observable quantity, including f_π and structure functions, is computed to be finite.

Gaussian models with generalized parton distributions $H(x, 0, Q^2)$ (see Eq. (26)) dominated by behavior near $x = 1$ present a set of examples that also yield a form factor with a $1/Q^2$ asymptotic behavior, and have an impact parameter distribution that is well behaved at each value of x for all b . The key asymptotic features are captured in the simple formula (76, 77): $H(x, 0, Q^2)_{x \rightarrow 1} = (1-x)^{n-1} e^{-a(1-x)^n Q^2}$, with $n > 2$ so that $q(x, b)_{x \rightarrow 1} = \frac{1}{2\pi a(1-x)} e^{-b^2/(4a(1-x)^n)}$. This form shows that $q(x, b)$ is well behaved for all values of b and for each value of x , but the integral over x contains a logarithmic divergence.

Relativistic light-front constituent quark models (78, 79, 75) that describe existing form factor data have a non-singular central charge density. These models can be most simply derived (79) by using the impulse approximation (evaluating the triangle diagram). One starts by evaluating the integral over the minus component of the loop momentum k^μ , and then cuts off the remaining integral over $x = k^+/p^+, k_\perp$ using a phenomenological wave function. The wave function of Ref. (75) is chosen to be a power-law form, and the resulting model describes the existing form factor data in the space-like region, f_π , and the transition form factor $f_{\pi\gamma}$ in which a virtual photon transforms a real pion into a real photon. The model form factor of (75) and the monopole fit of Eq. (37) are shown along with the measured data in Fig. 2. Both the fit and the model provide a good fit to the data, but present very different predictions for larger values of Q^2 where measurements remain to be done. The corresponding versions of $\rho(b)$ are shown in Fig. 3. The singularity of Eq. (38) is manifest as a rapidly rising function as b approaches zero, but the relativistic constituent quark model provides a smooth

function $\rho(b)$. The planned experiment (63) aims to achieve results up to $Q^2 = 6$ GeV². This should be large enough to resolve the differences between the model (75) and the monopole fit, or rule both out. However, this will probably not be sufficient to reach the regime where pQCD might be valid (63). The model (75) represents one useful phenomenology, but other interesting models exist. Computing the transverse density in those models would be useful.

4 NUCLEON TRANSVERSE CHARGE DENSITIES

In previous sections we have emphasized that a proper determination of a nucleon charge density requires a relation with the square of a field operator, and that this can be achieved through the transverse charge density (7,14,13,18,80), $\rho(b)$, given by Eq. (31). We review the first phenomenological analysis of existing data that determined $\rho(b)$ for the neutron and proton (18). The neutron results contradict the ancient idea, obtained from both meson-cloud and gluon-exchange models (81,82,83,84) regarding the positive value of the non-vanishing charge density at the center of the neutron. The meson-cloud idea is that the neutron sometimes undergoes a spontaneous quantum fluctuation into heavy proton surrounded by a negatively charged pionic cloud, leaving a positive central density(81). The quark-model mechanism (82,83,84) involves the repulsive nature of the one gluon exchange interaction between two d quarks.

These well-motivated physical considerations concern statements about the three-dimensional Fourier transform of the neutron's electric form factor $G_E^m(Q^2)$. However, such a transform is not the charge density. The only model-independent charge density is $\rho(b)$.

To proceed, recall the definitions of the form factors. With $J^\mu(x)$ as the elec-

tromagnetic current operator, in units of the proton charge, the nucleon form factors are given by

$$\langle p', \lambda' | J^\mu(0) | p, \lambda \rangle = \bar{u}(p', \lambda') \left(\gamma^\mu F_1(Q^2) + i \frac{\sigma^{\mu\alpha} q_\alpha}{2M} F_2(Q^2) \right) u(p, \lambda), \quad (42)$$

where the momentum transfer $q_\alpha = p'_\alpha - p_\alpha$ is taken as space-like, with $q^+ = 0$, so that $Q^2 \equiv -q^2 = \mathbf{q}^2 > 0$. The nucleon polarization states are chosen to be those of definite light-cone helicities λ, λ' (43) The charge (Dirac) form factor is F_1 , normalized such that $F_1(0)$ is the nucleon charge, and the magnetic (Pauli) form factor is F_2 , normalized such that $F_2(0)$ is the anomalous magnetic moment. The Sachs form factors(85)

$$G_E(Q^2) \equiv F_1(Q^2) - \frac{Q^2}{4M^2} F_2(Q^2), \quad G_M(Q^2) \equiv F_1(Q^2) + F_2(Q^2), \quad (43)$$

were introduced so as to provide an expression for the electron-nucleon cross section (in the one photon exchange approximation) that depends on the quantities G_E^2 and G_M^2 , but not the product $G_E G_M$. In the Breit frame, in which $\mathbf{p} = -\mathbf{p}'$, G_E is the nucleon helicity flip matrix element of J^0 . Furthermore, the scattering of neutrons from the electron cloud of atoms measures the derivative $-dG_E(Q^2)/dQ^2$ at $Q^2 = 0$, widely interpreted as six times the mean-square charge radius of the neutron. However, any probability or density interpretation of G_E is spoiled by a non-zero value of Q^2 , no matter how small. This is because the momentum difference between the initial and final states appears via the use of derivatives of momentum-conserving delta functions in the moments computed by Ref. (85). Any attempt to analytically incorporate relativistic corrections in a p^2/m_q^2 type of expansion would be doomed, by the presence of the quark mass, m_q , to be model-dependent. This is explained more thoroughly in Ref. (86).

We exploit Eq. (31) by using measured form factors to determine $\rho(b)$. Recent

parametrizations (87, 88, 89, 90, 91) of G_E and G_M are very useful, so we use Eq. (43) to obtain F_1 in terms of G_E, G_M . Then $\rho(b)$ can be expressed as a simple integral of known functions:

$$\rho(b) = \int_0^\infty \frac{dQ}{2\pi} Q J_0(Qb) \frac{G_E(Q^2) + \tau G_M(Q^2)}{1 + \tau}, \quad (44)$$

with $\tau = \frac{Q^2}{4M^2}$ and J_0 a cylindrical Bessel function.

A straightforward application of Eq. (44) to the proton using the parametrizations of Ref. (91) yields the results shown in the upper panel of Fig. 4. The curves obtained using the two different parametrizations overlap. Furthermore, there seems to be negligible sensitivity to form factors at very high values of Q^2 that are currently unmeasured. The density is peaked at low values of b , but has a long positive tail, suggesting a long-ranged, positively charged pion cloud.

The neutron results are shown in the lower panel of Fig. 4. The curves obtained using the two different parametrizations seem to overlap. The surprising result is that the central neutron charge density is negative. The values of the integral of Eq. (44) are somewhat sensitive to the regime $8 < Q^2 < 16 \text{ GeV}^2$ for which G_E is as yet unmeasured. About 30% of the value of $\rho(0)$ arises from this region. That $\rho(b=0) < 0$ was confirmed in Refs. (92, 80, 93, 94).

The negative central density deserves further explanation. See Fig. 4 in which the upper panel shows F_1 for the neutron from two parametrizations of Ref. (91). In both cases F_1 is negative (because of the dominance of the G_M term of Eq. (44)) for all values of Q^2 . This along with taking $b = 0$, $J_0(Qb) = 1$ in Eq. (44) leads immediately to the central negative result. The long range structure of the charge density is captured by displaying the quantity $b\rho(b)$ in the lower panel of Fig. 4. At very large distances from the center, $b\rho(b) < 0$ suggesting the existence of the long-ranged pion cloud. Thus the neutron transverse charge density has an

unusual behavior in which the positive charge density in the middle is sandwiched by negative charge densities at the inner and outer reaches of the neutron. A simple model in which the neutron fluctuates into a proton and a π^- parametrized to reproduce the negative-definite nature of the neutron's F_1 (95) reproduces the negative transverse central density. In this case, the negative nature arises from pions that penetrate to the center. The change from the nominal positive value obtained from G_E can be understood as originating in the boost to the infinite momentum frame (86).

One can gain information about the individual u and d quark densities by invoking charge symmetry (invariance under a rotation by π about the z (charge) axis in isospin space) (96,97,98,99) and neglecting effects of $s\bar{s}$ pairs (100).

Model independent information about nucleon structure is obtained, with the particular surprise that the central density of the neutron is negative. Future measurements of neutron electromagnetic form factors could render the present results more precise, or potentially modify them considerably. Obtaining a quantitative and intuitive understanding of these results presents a challenge to lattice QCD and to model builders.

4.1 Meaning of central density $b = 0$

The transverse coordinate $b = 0$ is the transverse center of the nucleon. It is of interest to note that, in the infinite momentum frame, this position is also the center of the nucleon. In that frame the nucleon has no longitudinal extent. This can be seen by considering a light cone wave function $\psi(x, \boldsymbol{\kappa})$. The canonically conjugate coordinate to $x = k^+/P^+$ is P^+x^- , (101) so that the coordinate-space wave function would depend on the product x^-P^+ . Thus when P^+ is infinite, the

coordinate-space wave function will vanish unless $x^- = 0$. This means that in the infinite momentum frame, the longitudinal density appears as a delta function and the position $b = 0$ is the true nucleon center (6).

4.2 Inclusive-exclusive Connection Interpretation of the negative neutron charge density

Generalized parton distributions (GPDs) contain information about the longitudinal momentum fraction x as well as the transverse position b . Information regarding these dependence's is obtained from experiment via GPDs that reproduce both deep inelastic scattering and elastic scattering data. Miller & Arrington (102) used this inclusive-exclusive connection to interpret the central neutron charge density, with the finding that the center of the neutron is dominated by negatively charged d quarks. Their argument is reviewed here.

The quantities $q(x, b)$ are not measured directly, but have been obtained from models that incorporate fits to parton distributions and electromagnetic nucleon form factors (103, 104, 105, 106). Form factor sum rules Eq. (26), Eq. (27) at zero skewness are exploited to model valence quark GPDs, $H_v^q \equiv H^q - H^{\bar{q}}$. This yields the net contribution to the form factors from quarks and anti-quarks. Possible effects of strangeness are neglected in these fits.

Each parametrization used (103, 104, 105) incorporates the Drell-Yan-West (107, 108) relationship between the behavior of the structure function $\nu W_2(x)$ function near $x = 1$, measured in inclusive reactions and the behavior of the electromagnetic form factor at large values of Q^2 , measured in the exclusive elastic scattering process. In particular, for a system of $n + 1$ valence quarks, described

by a power-law wave function

$$\lim_{x \rightarrow 1} \nu W_2(x) = (1-x)^{2n-1} \rightarrow \lim_{Q^2 \rightarrow \infty} F_1(Q^2) = \frac{1}{Q^{2n}}. \quad (45)$$

The value of n that defines the high- x behavior of the structure function also defines the high- Q^2 behavior of the form factor. This relation associates the behavior of large values of x with large momentum transfers, $Q^2 = \mathbf{q}^2$, which in turn corresponds to small values of b . There is a further connection between large values of x and small values of b which emerges from Eq. (11) and was seen in the example of Sect.1.3 (and Eq. (32)). If a single quark carries momentum fraction x very near unity, only one term in the sum of Eq. (11) survives and the restriction of this term to zero, causes the corresponding transverse coordinate to vanish. This interesting connection between different components of the position and momentum vectors is not associated with the uncertainty principle.

Given that the d quark dominates the large x quark-distribution function of the neutron, see *e.g.* (109), and that the central charge density of the neutron is negative, it is natural to conclude that the central charge density of the neutron arises from the predominance of d quarks at the center. This is shown in Fig. 6. One sees that for large values of x , b must be small to have a non-zero value of $\rho_n(x, b)$, and these non-zero values are negative.

4.3 Magnetization Density

We now try use transverse densities to obtain the nucleon magnetization density in the infinite momentum frame (110) in terms of a magnetization density. This quantity is closely related to the transverse charge density for a polarized nucleon obtained by Carlson and Vanderhaeghen (80). Our starting point is the relation that $\boldsymbol{\mu} \cdot \mathbf{B}$ is the matrix element of $\vec{J} \cdot \vec{A}$ in a definite state, $|X\rangle$.

Take the rest-frame magnetic field to be a constant vector in the 1 (or b_x) direction, and the corresponding vector potential as $\mathbf{A} = B b_y \hat{\mathbf{z}}$. Then consider the system in a frame in which the plus component of the momentum approaches infinity so that $\mathbf{J} \cdot \mathbf{A} \rightarrow J^+ A^-$. The anomalous magnetic moment may be extracted by taking the matrix element of $\boldsymbol{\mu} \cdot \mathbf{B}$ in the state

$$|X\rangle \equiv \frac{1}{\sqrt{2}} [|p^+, \mathbf{R} = \mathbf{0}, +\rangle + |p^+, \mathbf{R} = \mathbf{0}, -\rangle], \quad (46)$$

where $|p^+, \mathbf{R} = \mathbf{0}, +\rangle$ represents a transversely localized state of definite P^+ and light-cone helicity. The state $|X\rangle$ (14) may be interpreted as that of a transversely polarized target (111). The resulting anomalous magnetic moment μ_a is given by (110)

$$\mu_a = \langle X | \int d^2b b_y q_+^\dagger(0, \mathbf{b}) q_+(0, \mathbf{b}) | X \rangle, \quad (47)$$

where $q(x^-, \mathbf{b})$ is a quark-field operator, and $q_+ = \gamma^0 \gamma^+ q$. This matrix element is the anomalous magnetic moment because the use of the transversely localized state $|X\rangle$ and the factor b_y suppresses the Dirac contribution (111).

In Ref. (110) μ_a was evaluated by using Burkardt's (14) impact parameter distribution and then integrating by parts. The result was

$$\mu_a = \frac{1}{2M} \int d^2b \rho_M(b), \quad (48)$$

where

$$\rho_M(b) = \int \frac{d^2q}{(2\pi)^2} F_2(t = -\mathbf{q}^2) e^{-i\mathbf{q} \cdot \mathbf{b}}, \quad (49)$$

and the subscript M denotes the anomalous magnetic moment.

The expression (49) has an appealing simplicity. However, the directly-obtained Eq. (47) can also be evaluated immediately. We pursue this here to find

$$\mu_a = \frac{-1}{2M} \int d^2b b_y \frac{\partial \rho_M(b)}{\partial b_y}, \quad (50)$$

so that the quantity $-b_y \frac{\partial \rho_M(b)}{\partial b_y} \equiv \tilde{\rho}_M(\mathbf{b})$ also has an interpretation as an anomalous magnetization density. The two integrals appearing in Eq. (48) and Eq. (50) the same value. Ref. (110) rejected the use of $\tilde{\rho}_M(\mathbf{b})$ as a magnetization density because of the appearance of an explicit direction y . However, this direction has a general interpretation as the transverse direction orthogonal to that of the transverse magnetic field. We evaluate $\tilde{\rho}_M(\mathbf{b})$ in terms of $F_2(Q^2)$ to find

$$\tilde{\rho}_M(\mathbf{b}) = \sin^2 \phi b \int_0^\infty \frac{q^2 dq}{2\pi} J_1(qb) F_2(q^2), \quad (51)$$

where ϕ is the angle between the direction of \mathbf{b} and that of the transverse magnetic field, which is also the direction of the nucleon polarization. Thus the physical direction of the polarization or magnetic field provides a definite spatial direction. Indeed the magnetization density $\tilde{\rho}_M(\mathbf{b})$ is largest in directions perpendicular to the direction of the nucleonic polarization (or magnetic field), as shown in Fig. 7. The largest values occur for $\phi = \pi/2$, and the magnetization density peaks at about 0.5 fm. Furthermore $\tilde{\rho}_M(\mathbf{b})$ vanishes if $b = 0$ or if $\phi = 0$. These features are in accord with the expectations of classical physics. A current in the z direction causes a magnetic dipole density $\sim \mathbf{r} \times \vec{J}$ in the x -direction for positions \mathbf{r} along the y -direction. Therefore we conclude here that the quantity $\tilde{\rho}_M(\mathbf{b})$ is the preferred expression for the magnetization density.

Hoyer & Kurki have computed the transverse density of the electron (112). Using their expression for the electron F_2 in Eq. (50) leads to the correct result for the electron's anomalous magnetic moment, μ_a^e . Furthermore the presence of the $\sin^2 \phi$ term is consistent with their physical interpretation of the sign of μ_a^e as caused by currents in the positive (negative) z - direction for positive (negative) values of y . Computing the cross product between \mathbf{b} and those currents gives magnetization in the x -direction for both positive and negative values of y .

To better understand this new magnetization density, consider the moments of both densities. Define the n th moment of ρ_M as

$$\langle b^{2n} \rangle_M \equiv \int d^2b b^{2n} \rho_M(b). \quad (52)$$

These quantities are related to the n th derivative of $F_2(q^2)$. Similarly the n th moment of $\tilde{\rho}_M$ is given by

$$\langle b^{2n} \rangle_{\tilde{M}} \equiv - \int d^2b b^{2n} b_y \frac{\partial \rho_M(b)}{\partial b_y}. \quad (53)$$

Then use of Eq. (49) and integration by parts shows that

$$\langle b^{2n} \rangle_{\tilde{M}} = (n + 1) \langle b^{2n} \rangle_M. \quad (54)$$

The $n = 0$ moment corresponds to the anomalous magnetic moment which is the same for the two densities. The case $n = 1$ which defines the mean-square magnetic radius is more interesting. Ref. (110) showed that $\langle b^2 \rangle_M$ was slightly larger than $\langle b^2 \rangle_{Ch}$ (which is obtained from F_1). However $\langle b^2 \rangle_{\tilde{M}}$ is twice as large as $\langle b^2 \rangle_M$ and therefore is much larger than $\langle b^2 \rangle_{Ch}$! This clearly shows that the proton's magnetization density extends much further than its charge density, a conclusion obtained in Ref. (110). This is surprising because it contradicts simple naive intuition gained from the rapid fall of the ratio G_E/G_M with increasing momentum transfer (3), if one assumes that G_E (G_M) is related to the spatial extent of the charge (magnetization) density.

4.4 Non-cylindrically symmetric transverse charge density and shape of the nucleon

Carlson and Vanderhaeghen (80) computed the transverse charge density $\rho_T^N(\mathbf{b})$ in a given state of transverse polarization. For the case that the polarization is in

the x direction their result is expressed as

$$\rho_T^N(\mathbf{b}) = \rho(b) + \sin \phi \int_0^\infty \frac{dQ}{2\pi} \frac{Q^2}{2M} J_1(bQ) F_2(Q^2), \quad (55)$$

where $\rho(b)$ is obtained from Eq. (31). The sign of the second term of Eq. (55) is obtained using the definition that \mathbf{q} is the momentum absorbed by the target nucleon. Their results for the proton are shown in Fig. 8.

The magnetization density $\tilde{\rho}_M(\mathbf{b})$ presented here and the transverse charge density of Ref. (80) each depend on the direction of \mathbf{b} , thus indicating a non-spherical shape of the nucleon or the violation of cylindrical symmetry. These violations of cylindrical symmetry should not be confused with those present in earlier papers on the shape of the nucleon Refs. (113,114,51) that define a shape via the matrix elements of a spin-dependent density operator. The transverse charge densities that are the main subject of this article are matrix elements of currents that are local in transverse coordinate space and are related to GPDs. In contrast, those shapes of (113,114,51), computed from momentum-space wave functions and probabilities are matrix elements of quark densities for given values of transverse momenta and are related to TMDs. It should also be noted that the first example of (113) is presented in coordinate space. The infinite momentum frame version of the spin-dependent density operator is $q_+^\dagger(0, \mathbf{b}) \frac{1}{2}(1 + \mathbf{n} \cdot \boldsymbol{\gamma}) q_+(0, \mathbf{b})$, where \mathbf{n} is an arbitrary transverse direction (49). Evaluating the matrix element of this quantity produces the spin-dependent density, which can be thought of as the x^- integrated version of the coordinate space results of (113). The proton is non-spherical if the function \tilde{A}_{T10}'' of (50) is non-vanishing, as recent lattice calculations show (115). One can also examine several different generalized densities $q_+^\dagger(0, \mathbf{b}) \Gamma q_+(0, \mathbf{b})$, with operators Γ denoted in (49).

5 TRANSVERSE TRANSITION CHARGE DENSITIES

There is much experimental interest in measuring transition form factors that represent probability amplitudes for a nucleon undergoing electron scattering to make a transition to a given baryon resonance. Substantial experimental efforts are underway at electron-scattering laboratories such as Jefferson Laboratory, ELSA in Bonn, and MAMI in Mainz. Moreover, there is considerable interest in using lattice techniques to make QCD calculations of these transition amplitudes.

Carlson & Vanderhaeghen (80) used empirical information regarding the $N \rightarrow \Delta$ transition form factors to map out the transition charge density. This, in a transversely polarized N and Δ , contains monopole, dipole and quadrupole patterns. The latter corresponds to a deformation of the nucleon and Δ transverse charge density. Substantial deformations are observed. Lattice QCD calculations have been applied to these very same transition densities (47,48). The Δ^+ charge density is found to be elongated along the axis of the spin and the quadrupole moment is larger than the value characterizing a point particle. This means the the Δ^+ is prolately deformed.

Tiator & Vanderhaeghen (116) used recent experimental data to analyze the electromagnetic transition from the nucleon to the $P_{11}(1440)$ resonance, which is often believed to be the first radial excitation of the proton. They used the empirical transition form factors to find that the transition from the proton to the $P_{11}(1440)$ is dominated by up quarks in a central region of width of about 0.5 fm and by down quarks in an outer band which extends up to about 1 fm. Tiator *et al.* (117) are extending the study of transition transverse densities to the S_{11} and D_{13} resonances.

6 NUCLEAR TRANSVERSE CHARGE DENSITIES

The very same infinite momentum frame formalism can be applied to the analysis of nuclear form factors. The non-relativistic approximation of Eq. (6) is generally applicable for existing measurements of nuclear form factors (6). However, meson exchange currents are known to be important for $Q^2 > 2 \text{ GeV}^2$ (118). In that case, the charged constituents have different masses (see Eq. (7)), the pion moves relativistically, and the charge density is not a three-dimensional Fourier transform of the electromagnetic form factor. Moreover, Jefferson Laboratory plans to considerably extend the available range of momentum transfer for light nuclear form factors. Hence transverse charge densities which supply model independent information are of considerable relevance for nuclear physics.

Carlson & Vanderhaeghen (119) made the first computation of a nuclear transverse density in their analysis of the deuteron empirical transverse charge densities (120). The charge densities are characterized by monopole, dipole and quadrupole patterns because the deuteron has a spin of unity. Ref. (119) observes a dip in the center-of-charge density for helicity-zero deuterons. This central depression is in accord with standard nuclear force model calculations (121) and is a simple consequence of the deuteron D -state. We note that the deuteron is a non-relativistic system in the sense defined by Ref. (6). Thus these densities can, with a high degree of accuracy, be thought of as an integral over z of the corresponding non-relativistic density; see Eq. (15). The dip is an important finding, because it is model independent. Ref. (119) also finds that transversely polarized deuterons show dipole and quadrupole structure in the charge densities. Their electric dipole and quadrupole moments only depend on the spin-1 particle's anomalous magnetic dipole moment and its anomalous electric quadrupole moment, arising

from its internal structure.

Nuclei are non-relativistic systems (6) so that for presently available data the principle distinction between transverse densities and the usual three-dimensional Fourier transform is that the former is an integral Eq. (15) over the latter. However, existing nuclear data extend only to about $Q^2 = 1 \text{ GeV}^2$ (122, 123, 124). In this case the motion of the nucleons within the nucleus is just barely relativistic. If, as expected, data are taken at higher values of Q^2 relativistic effects can be expected to be important. One example is the nuclei with $A = 3$ and mass M_3 and Sachs electric and magnetic form factors F_C, F_M (122). If $Q^2/4M_3^2$ is of order unity, the distinction between $F_1 = F_C - Q^2/4M_3^2 F_M$ and F_C will become important and the role of transverse densities may become very important.

6.1 Other Applications

Transverse momentum densities, giving the momentum density of hadrons, have also been studied (125, 126). The spatial distribution of the momentum component P^+ is found to be related to Fourier transforms of gravitational form factors (125) which in turn are related to experimentally observed data. This is because gravitational form factors are matrix elements of the energy-momentum tensor obtainable as second Mellin moments of GPDs (127, 25, 128). The proton momentum density in the transverse plane was found to be more compact than its charge density (125).

Any charge density will deform when subjected to an external electric field; related measurable quantities are called polarizabilities. Gorchtein *et al.* (129) extended the transverse charge density formalism to extract light-front quark charge densities related to polarizabilities and showed that the resulting induced

polarizations can be extracted from proton generalized polarizabilities (130,131). The available data for the generalized electric polarizabilities of the proton yield a transverse density that shows an usual oscillatory pattern.

7 SUMMARY AND FUTURE DIRECTIONS

Transverse charge densities are a new tool for analyzing electromagnetic form factors of systems composed of constituents that move relativistically. These quantities are hadronic charge densities as seen in a reference frame moving with infinite momentum. One of the main advantages of the infinite momentum framework is that boosts in the transverse direction form a kinematic subgroup of the Poincaré group, so that transformations to frames moving in a direction transverse to that of the infinite momentum are carried out using the transverse position operator. This is just like the usual non-relativistic Galilean transformation. Thus the two-dimensional Fourier transformation of electromagnetic form factors provides a rigorous way to study charge and magnetization densities. Transverse charge densities involve matrix elements of local operators $q_+^\dagger(t=0, z=0, \mathbf{b})\Gamma q_+(t=0, z=0, \mathbf{b})$, computable using any of the light-front, equal-time or lattice techniques.

The use of transverse momentum densities has led to some very interesting findings. Examples include the negative nature of the central neutron charge density (18) as caused by the dominance of d quarks at the center (102), the seemingly singular nature of the density at the center of the pion (17), the spatial extent of the proton's magnetization density is greater than that of its charge density (110), and the deformation of the nucleon (113,115) and the Δ baryon (80) is substantial. The positive sign of the electron anomalous magnetic moment

is explained (112).

Transverse densities have been used to analyze other baryon transitions (116), nuclear charge densities (119) momentum densities (128) and generalized polarizabilities (129).

Measurements of form factors at larger values of Q^2 than are presently available is needed to test the singularity of the pionic transverse density and the inner core of the neutron transverse density. It also seems likely that the use of transverse charge densities will become the chosen tool to analyze nuclear charge distributions once very high-momentum transfer data become available. Transverse densities are relevant whenever matrix elements of an operator $q_+^\dagger(t = 0, z = 0, \mathbf{b})\Gamma q_+(t = 0, z = 0, \mathbf{b})$ appears. Thus one may expect to see a host of interesting, informative and important future applications of transverse densities.

8 ACKNOWLEDGMENTS

This work is partially supported by the USDOE. I thank J. Arrington, A. Bernstein, M. Burkardt, C. Carlson, I. Cloët, P. Hoyer, E. Piasetzky, G. Ron, A. Radyushkin, J. Rinehimer, B. Tiburzi, M. Vanderhaeghen and L. Zhu for useful discussions regarding transverse charge distributions.

LITERATURE CITED

1. H.-y. Gao, *Int. J. Mod. Phys.* **E12**, 1 (2003), nucl-ex/0301002.
2. C. E. Hyde and K. de Jager, *Ann. Rev. Nucl. Part. Sci.* **54**, 217 (2004), nucl-ex/0507001.
3. C. F. Perdrisat, V. Punjabi, and M. Vanderhaeghen, *Prog. Part. Nucl. Phys.* **59**, 694 (2007), hep-ph/0612014.

4. J. Arrington, C. D. Roberts, and J. M. Zanotti, *J. Phys.* **G34**, S23 (2007), nucl-th/0611050.
5. R. Hofstadter, *Rev. Mod. Phys.* **28**, 214 (1956).
6. G. A. Miller, *Phys. Rev.* **C80**, 045210 (2009), 0908.1535.
7. D. E. Soper, *Phys. Rev.* **D15**, 1141 (1977).
8. N. Nakanishi, *Prog. Theor. Phys. Suppl.* **43**, 1 (1969).
9. N. Nakanishi, *Prog. Theor. Phys. Suppl.* **95**, 1 (1988).
10. J. Carbonell, V. A. Karmanov, and M. Mangin-Brinet, *Eur. Phys. J.* **A39**, 53 (2009), 0809.3678.
11. G. A. Miller and B. C. Tiburzi, (2009), 0911.3691.
12. L. Susskind, *Phys. Rev.* **165**, 1547 (1968).
13. M. Diehl, *Eur. Phys. J.* **C25**, 223 (2002), hep-ph/0205208.
14. M. Burkardt, *Int. J. Mod. Phys.* **A18**, 173 (2003), hep-ph/0207047.
15. M. Burkardt, *Phys. Rev.* **D62**, 071503 (2000), hep-ph/0005108.
16. M. Diehl, T. Feldmann, R. Jakob, and P. Kroll, *Nucl. Phys.* **B596**, 33 (2001), hep-ph/0009255.
17. G. A. Miller, *Phys. Rev.* **C79**, 055204 (2009), 0901.1117.
18. G. A. Miller, *Phys. Rev. Lett.* **99**, 112001 (2007), 0705.2409.
19. R. J. Glauber and G. Matthiae, *Nucl. Phys.* **B21**, 135 (1970).
20. M. Luzum and P. Romatschke, *Phys. Rev. Lett.* **103**, 262302 (2009), 0901.4588.
21. J. F. Gunion, S. J. Brodsky, and R. Blankenbecler, *Phys. Rev.* **D8**, 287 (1973).
22. G. P. Lepage and S. J. Brodsky, *Phys. Rev.* **D22**, 2157 (1980).
23. J. Carbonell, B. Desplanques, V. A. Karmanov, and J. F. Mathiot, *Phys.*

- Rept. **300**, 215 (1998), nucl-th/9804029.
24. D. Mueller, D. Robaschik, B. Geyer, F. M. Dittes, and J. Horejsi, *Fortschr. Phys.* **42**, 101 (1994), hep-ph/9812448.
25. X.-D. Ji, *Phys. Rev.* **D55**, 7114 (1997), hep-ph/9609381.
26. A. V. Radyushkin, *Phys. Rev.* **D56**, 5524 (1997), hep-ph/9704207.
27. J. C. Collins, L. Frankfurt, and M. Strikman, *Phys. Rev.* **D56**, 2982 (1997), hep-ph/9611433.
28. X.-D. Ji, *J. Phys.* **G24**, 1181 (1998), hep-ph/9807358.
29. A. V. Radyushkin, (2000), hep-ph/0101225.
30. K. Goeke, M. V. Polyakov, and M. Vanderhaeghen, *Prog. Part. Nucl. Phys.* **47**, 401 (2001), hep-ph/0106012.
31. M. Diehl, *Phys. Rept.* **388**, 41 (2003), hep-ph/0307382.
32. X. Ji, *Ann. Rev. Nucl. Part. Sci.* **54**, 413 (2004).
33. A. V. Belitsky and A. V. Radyushkin, *Phys. Rept.* **418**, 1 (2005), hep-ph/0504030.
34. P. Hagler, *Phys. Lett.* **B594**, 164 (2004), hep-ph/0404138.
35. S. Boffi and B. Pasquini, *Riv. Nuovo Cim.* **30**, 387 (2007), 0711.2625.
36. J. C. Collins and D. E. Soper, *Nucl. Phys.* **B194**, 445 (1982).
37. J. P. Ralston and D. E. Soper, *Nucl. Phys.* **B152**, 109 (1979).
38. V. M. Belyaev and B. L. Ioffe, *Nucl. Phys.* **B313**, 647 (1989).
39. M. Anselmino, A. Efremov, and E. Leader, *Phys. Rept.* **261**, 1 (1995), hep-ph/9501369.
40. P. J. Mulders and R. D. Tangerman, *Nucl. Phys.* **B461**, 197 (1996), hep-ph/9510301.
41. B. Chibisov and A. R. Zhitnitsky, *Phys. Rev.* **D52**, 5273 (1995), hep-

- ph/9503476.
42. B. Pasquini, S. Boffi, A. V. Efremov, and P. Schweitzer, (2009), 0912.1761.
 43. J. B. Kogut and D. E. Soper, Phys. Rev. **D1**, 2901 (1970).
 44. X.-d. Ji, Phys. Rev. Lett. **91**, 062001 (2003), hep-ph/0304037.
 45. A. V. Belitsky, X. Ji, and F. Yuan, Nucl. Phys. **B656**, 165 (2003), hep-ph/0208038.
 46. W. Broniowski, S. Prelovsek, L. Santelj, and E. R. Arriola, (2009), 0911.4705.
 47. C. Alexandrou *et al.*, Phys. Rev. **D79**, 014507 (2009), 0810.3976.
 48. C. Alexandrou *et al.*, Nucl. Phys. **A825**, 115 (2009), 0901.3457.
 49. M. Diehl and P. Hagler, Eur. Phys. J. **C44**, 87 (2005), hep-ph/0504175.
 50. QCDSF, M. Gockeler *et al.*, Phys. Rev. Lett. **98**, 222001 (2007), hep-lat/0612032.
 51. G. A. Miller, Phys. Rev. **C76**, 065209 (2007), 0708.2297.
 52. G. P. Lepage and S. J. Brodsky, Phys. Lett. **B87**, 359 (1979).
 53. G. R. Farrar and D. R. Jackson, Phys. Rev. Lett. **43**, 246 (1979).
 54. V. L. Chernyak, V. G. Serbo, and A. R. Zhitnitsky, Sov. J. Nucl. Phys. **31**, 552 (1980).
 55. A. V. Efremov and A. V. Radyushkin, Theor. Math. Phys. **42**, 97 (1980).
 56. V. L. Chernyak and A. R. Zhitnitsky, Phys. Rept. **112**, 173 (1984).
 57. H.-n. Li and G. Stermann, Nucl. Phys. **B381**, 129 (1992).
 58. E. Braaten and S.-M. Tse, Phys. Rev. **D35**, 2255 (1987).
 59. G. A. Miller and J. Pasupathy, Z. Phys. **A348**, 123 (1994).
 60. A. V. Radyushkin, Nucl. Phys. **A532**, 141 (1991).
 61. Jefferson Lab, H. P. Blok *et al.*, Phys. Rev. **C78**, 045202 (2008), 0809.3161.

62. Jefferson Lab, G. M. Huber *et al.*, Phys. Rev. **C78**, 045203 (2008), 0809.3052.
63. Jefferson Laboratory Proposal E12-6-101, G. M. Huber *et al.*
64. M. L. Goldberger, D. E. Soper, and A. H. Guth, Phys. Rev. **D14**, 2633 (1976).
65. S. J. Brodsky and G. F. de Teramond, Phys. Rev. **D77**, 056007 (2008), 0707.3859.
66. H. J. Kwee and R. F. Lebed, JHEP **01**, 027 (2008), 0708.4054.
67. H. R. Grigoryan and A. V. Radyushkin, Phys. Rev. **D76**, 115007 (2007), 0709.0500.
68. W. Broniowski, E. R. Arriola, and K. Golec-Biernat, AIP Conf. Proc. **1030**, 286 (2008), 0804.0718.
69. E. Ruiz Arriola and W. Broniowski, Phys. Rev. **D67**, 074021 (2003), hep-ph/0301202.
70. W. Broniowski and E. Ruiz Arriola, Phys. Lett. **B574**, 57 (2003), hep-ph/0307198.
71. P. Brauel *et al.*, Zeit. Phys. **C3**, 101 (1979).
72. H. Ackermann *et al.*, Nucl. Phys. **B137**, 294 (1978).
73. NA7, S. R. Amendolia *et al.*, Nucl. Phys. **B277**, 168 (1986).
74. T. Horn *et al.*, Phys. Rev. **C78**, 058201 (2008), 0707.1794.
75. C.-W. Hwang, Phys. Rev. **D64**, 034011 (2001), hep-ph/0105016.
76. A. V. Radyushkin, Phys. Rev. **D58**, 114008 (1998), hep-ph/9803316.
77. M. Burkardt and G. A. Miller, Phys. Rev. **D74**, 034015 (2006), hep-ph/0312190.
78. P. L. Chung, F. Coester, and W. N. Polyzou, Phys. Lett. **B205**, 545 (1988).

79. T. Frederico and G. A. Miller, Phys. Rev. **D45**, 4207 (1992).
80. C. E. Carlson and M. Vanderhaeghen, Phys. Rev. Lett. **100**, 032004 (2008), 0710.0835.
81. A. W. Thomas, S. Theberge, and G. A. Miller, Phys. Rev. **D24**, 216 (1981).
82. J. L. Friar, Part.Nucl. **4**, 153 (1972).
83. R. D. Carlitz, S. D. Ellis, and R. Savit, Phys. Lett. **B68**, 443 (1977).
84. N. Isgur, G. Karl, and D. W. L. Sprung, Phys. Rev. **D23**, 163 (1981).
85. R. G. Sachs, Phys. Rev. **126**, 2256 (1962).
86. J. A. Rinehimer and G. A. Miller, Phys. Rev. **C80**, 015201 (2009), 0902.4286.
87. R. Bradford, A. Bodek, H. S. Budd, and J. Arrington, Nucl. Phys. Proc. Suppl. **159**, 127 (2006), hep-ex/0602017.
88. J. J. Kelly, Phys. Rev. **C70**, 068202 (2004).
89. J. Arrington, Phys. Rev. **C69**, 022201 (2004), nucl-ex/0309011.
90. J. Arrington, W. Melnitchouk, and J. A. Tjon, Phys. Rev. **C76**, 035205 (2007), 0707.1861.
91. W. M. Alberico, S. M. Bilenky, C. Giunti, and K. M. Graczyk, Phys. Rev. **C79**, 065204 (2009), 0812.3539.
92. B. Pasquini and S. Boffi, Phys. Rev. **D76**, 074011 (2007), 0707.2897.
93. S. Boffi and B. Pasquini, Mod. Phys. Lett. **A24**, 2882 (2009), 0910.1186.
94. D. S. Hwang, D. S. Kim, and J. Kim, Phys. Lett. **B669**, 345 (2008), 0805.4773.
95. J. A. Rinehimer and G. A. Miller, Phys. Rev. **C80**, 025206 (2009), 0906.5020.
96. G. A. Miller, A. W. Thomas, and A. G. Williams, Phys. Rev. Lett. **56**, 2567

- (1986).
97. G. A. Miller, B. M. K. Nefkens, and I. Slaus, *Phys. Rept.* **194**, 1 (1990).
 98. G. A. Miller, *Phys. Rev.* **C57**, 1492 (1998), nucl-th/9711036.
 99. G. A. Miller, A. K. Opper, and E. J. Stephenson, *Ann. Rev. Nucl. Part. Sci.* **56**, 253 (2006), nucl-ex/0602021.
 100. HAPPEX, A. Acha *et al.*, *Phys. Rev. Lett.* **98**, 032301 (2007), nucl-ex/0609002.
 101. H. J. Pirner and N. Nurpeissov, *Phys. Lett.* **B595**, 379 (2004), hep-ph/0404179.
 102. G. A. Miller and J. Arrington, *Phys. Rev.* **C78**, 032201 (2008), 0806.3977.
 103. M. Guidal, M. V. Polyakov, A. V. Radyushkin, and M. Vanderhaeghen, *Phys. Rev.* **D72**, 054013 (2005), hep-ph/0410251.
 104. M. Diehl, T. Feldmann, R. Jakob, and P. Kroll, *Eur. Phys. J.* **C39**, 1 (2005), hep-ph/0408173.
 105. S. Ahmad, H. Honkanen, S. Liuti, and S. K. Taneja, *Phys. Rev.* **D75**, 094003 (2007), hep-ph/0611046.
 106. B. C. Tiburzi, W. Detmold, and G. A. Miller, *Phys. Rev.* **D70**, 093008 (2004), hep-ph/0408365.
 107. S. D. Drell and T.-M. Yan, *Phys. Rev. Lett.* **24**, 181 (1970).
 108. G. B. West, *Phys. Rev. Lett.* **24**, 1206 (1970).
 109. J. Pumplin *et al.*, *JHEP* **07**, 012 (2002), hep-ph/0201195.
 110. G. A. Miller, E. Piasetzky, and G. Ron, *Phys. Rev. Lett.* **101**, 082002 (2008), 0711.0972.
 111. M. Burkardt, *Phys. Rev.* **D72**, 094020 (2005), hep-ph/0505189.
 112. P. Hoyer and S. Kurki, (2009), 0911.3011.

113. G. A. Miller, Phys. Rev. **C68**, 022201 (2003), nucl-th/0304076.
114. A. Kvinikhidze and G. A. Miller, Phys. Rev. **C73**, 065203 (2006), nucl-th/0603035.
115. QCDSF, G. Schierholz, Workshop on Transverse partonic Structure of Hadrons,2009 (2009).
116. L. Tiator and M. Vanderhaeghen, Phys. Lett. **B672**, 344 (2009), 0811.2285.
117. L. Tiator, D. Drechsel, S. S. Kamalov, and M. Vanderhaeghen, (2009), 0909.2335.
118. D. O. Riska, In Rho M, Wilkinson D: Mesons In Nuclei, Vol.I, Amsterdam 1979, 755-787.
119. C. E. Carlson and M. Vanderhaeghen, Eur. Phys. J. **A41**, 1 (2009), 0807.4537.
120. JLAB t20, D. Abbott *et al.*, Eur. Phys. J. **A7**, 421 (2000), nucl-ex/0002003.
121. J. L. Forest *et al.*, Phys. Rev. **C54**, 646 (1996), nucl-th/9603035.
122. A. Amroun *et al.*, Nucl. Phys. **A579**, 596 (1994).
123. I. Sick, Progress in Particle and Nuclear Physics **47**, 245 (2001).
124. I. Sick, Phys. Rev. **C77**, 041302 (2008).
125. Z. Abidin and C. E. Carlson, Phys. Rev. **D78**, 071502 (2008), 0808.3097.
126. O. V. Selyugin and O. V. Teryaev, Phys. Rev. **D79**, 033003 (2009), 0901.1786.
127. X.-D. Ji, Phys. Rev. Lett. **78**, 610 (1997), hep-ph/9603249.
128. Z. Abidin and C. E. Carlson, Phys. Rev. **D77**, 095007 (2008), 0801.3839.
129. M. Gorchtein, C. Lorce, B. Pasquini, and M. Vanderhaeghen, (2009), 0911.2882.
130. P. A. M. Guichon, G. Q. Liu, and A. W. Thomas, Nucl. Phys. **A591**, 606

(1995), nucl-th/9605031.

131. D. Drechsel, G. Knochlein, A. Y. Korchin, A. Metz, and S. Scherer, Phys. Rev. **C57**, 941 (1998), nucl-th/9704064.

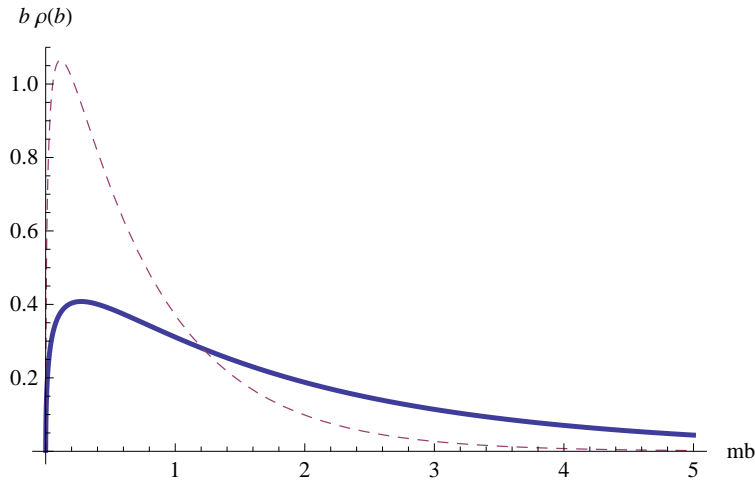


Figure 1: $b\rho(b)$ for the model of Eq. (20). Solid $\epsilon = 0.01$, dashed $\epsilon = 0.1$.

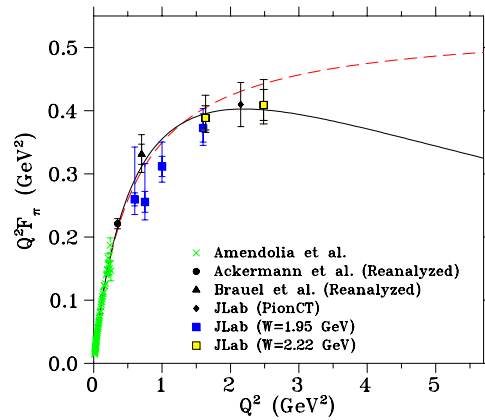


Figure 2: Pion form factor data as plotted in (62). The data labeled Jlab are from (62). The data Brauel *et al.* (71) and that of Ackermann *et al.* (72) have using the method of (62). The Amendola data *et al.* are from (73) The data point labeled PionCT is from (74). The (red) dashed curve uses the monopole fit Eq. (37) and the (black) solid line the constituent quark model of (75). $b\rho(b)$ for the model of Eq. (20). Reprinted from Ref. (17) with permission of the APS.

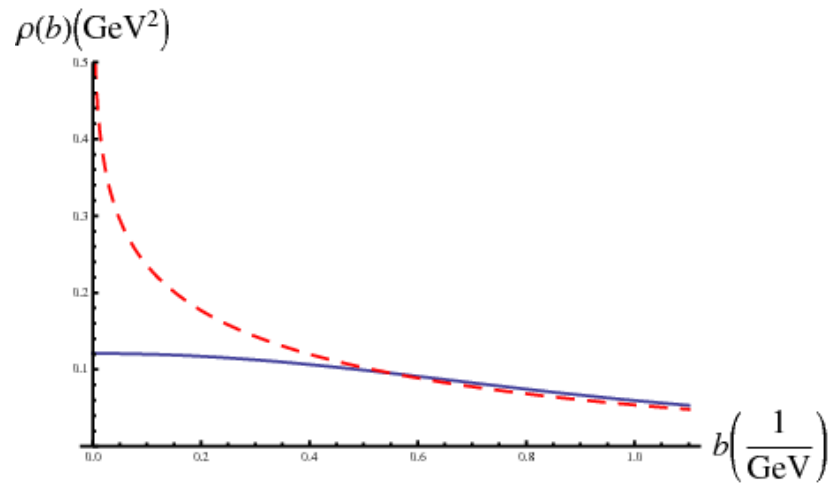


Figure 3: $\rho(b)$ corresponding to the two models shown in Fig. 2. The (red) dashed curve represents the transverse density obtained from the monopole fit and the (blue) solid-line is obtained using the relativistic constituent quark model of(75). Reprinted from Ref. (17) with permission of the APS.

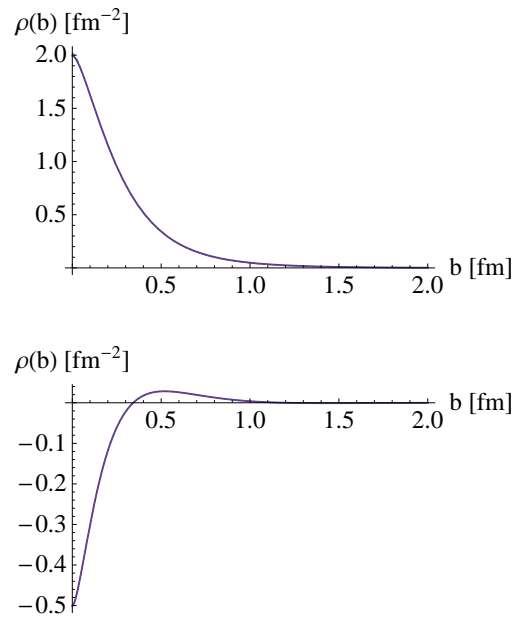


Figure 4: Nucleon $\rho(b)$ Upper panel: proton transverse charge density. Lower panel: neutron transverse charge density. These densities are obtained using the parametrization of (91).

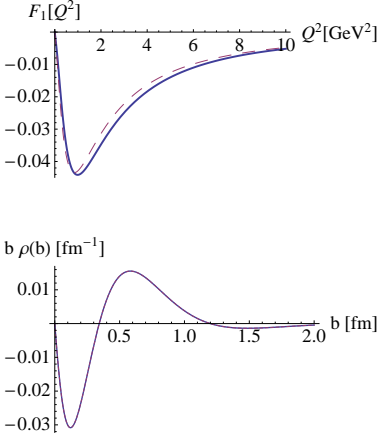


Figure 5: Neutron F_1 and $b\rho(b)$. Upper panel: $F_1(Q^2)$. Lower panel: $b\rho(b)$. The solid curves are obtained using Fit 1 and the dashed curves with Fit 2 of $\rho_n(x,b)$ (91).

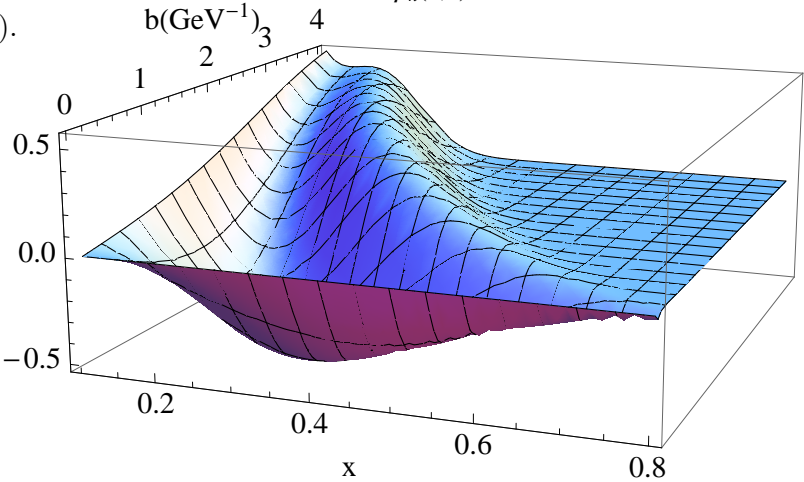


Figure 6: Neutron impact parameter charge distributions, $\rho_n(x, b)$ as a function of b .

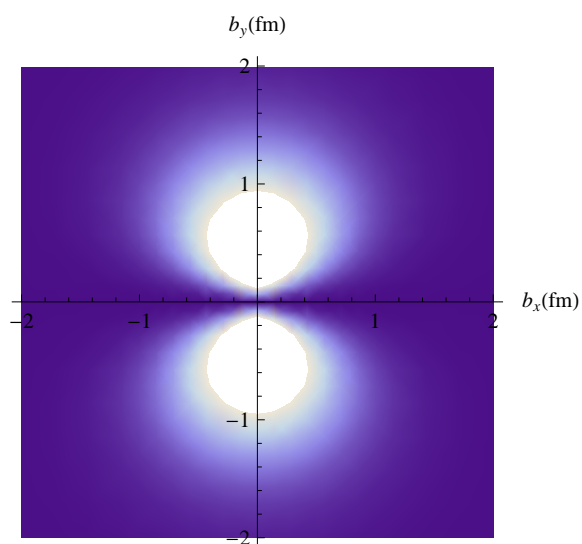
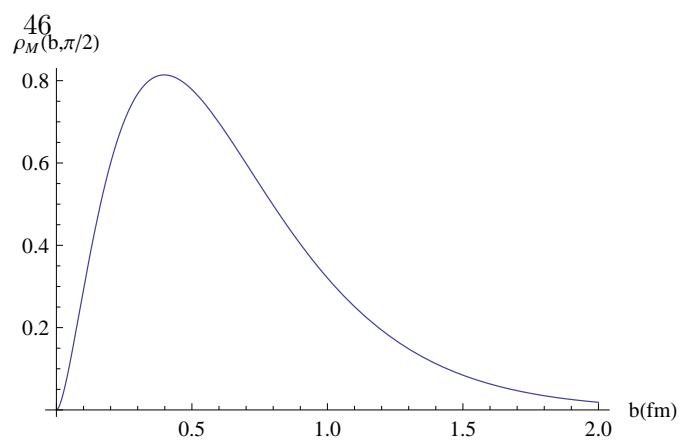


Figure 7: Upper panel: $\tilde{\rho}_M(\mathbf{b} = (b, \phi = \pi/2))$ as a function of b . Lower panel: Density plot of $\tilde{\rho}_M(\mathbf{b})$. The horizontal axis is the direction of the applied magnetic field. The largest (smallest) values of $\tilde{\rho}_M$ are denoted by the brightest (darkest) areas. This figure is obtained using a dipole parametrization for F_2 of the proton.

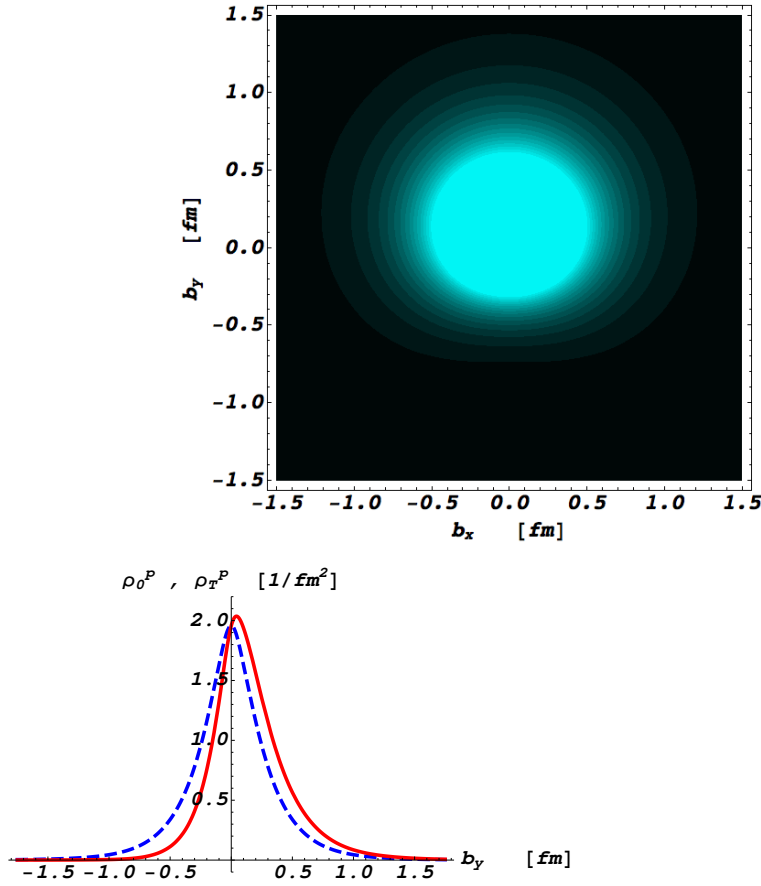


Figure 8: Quark transverse charge densities in the proton, after (80), figure provided courtesy of M. Vanderhaeghen. The upper panel shows the density in the transverse plane for a proton polarized along the x -axis. The light (dark) regions correspond with largest (smallest) values of the density. The lower panel compares the density along the y -axis for an unpolarized proton (dashed curve), and for a proton polarized along the x -axis (solid curve). The proton form factors are from Arrington *et al.* (90). The momentum transfer \mathbf{q} is the momentum added to the target proton.

